Rapid Communications

Magnon decay theory of Gilbert damping in metallic antiferromagnets

Haakon T. Simensen, Akashdeep Kamra, Roberto E. Troncoso, and Arne Brataas
Center for Quantum Spintronics, Department of Physics, Norwegian University of Science and Technology, NO-7491 Trondheim, Norway

(Received 26 June 2019; revised manuscript received 25 November 2019; published 9 January 2020)

Gilbert damping is a key property governing magnetization dynamics in ordered magnets. We present a theoretical study of intrinsic Gilbert damping induced by magnon decay in antiferromagnetic metals through *s-d* exchange interaction. Our theory delineates the qualitative features of damping in metallic antiferromagnets owing to their bipartite nature. It provides analytic expressions for the damping parameters yielding values consistent with recent first-principles calculations. Magnon-induced intraband electron scattering is found to predominantly cause magnetization damping, whereas the Néel field is found to be damped via disorder. Depending on the conduction electron band structure, we predict that magnon-induced interband electron scattering around band crossings may be exploited to engineer a strong Néel field damping.

DOI: 10.1103/PhysRevB.101.020403

Introduction. The dynamical properties of a harmonic mode are captured by its frequency and lifetime [1,2]. While the eigenfrequency is typically determined by the linearized equations of motion, or equivalently by a noninteracting description of the corresponding quantum excitation, the lifetime embodies rich physics stemming from its interaction with one or more dissipative baths [1,3]. Dissipation plays a central role in the system response time. In the context of magnetic systems employed as memories, the switching times decrease with increasing damping thereby requiring a stronger dissipation for fast operation [4–6]. The dissipative properties of the system also result in rich phenomena such as quantum phase transitions [7–10]. Furthermore, the formation of hybrid excitations, such as magnon-polarons [11–18] and magnon-polaritons [19–24], requires the dissipation to be weak with respect to the coupling strengths between the two participating excitations [25]. Therefore, in several physical phenomena that have emerged in recent years [12,16,26–30], damping not only determines the system response but also the very nature of the eigenmodes themselves. Understanding, exploiting, and controlling the damping in magnets is thus a foundational pillar of the field.

The success of Landau-Lifshitz-Gilbert (LLG) phenomenology [31,32] in describing ferromagnetic dynamics has inspired vigorous efforts towards obtaining the Gilbert damping parameter using a wide range of microscopic theories. The quantum particles corresponding to magnetization dynamics—magnons—provide one such avenue for microscopic theories and form the central theme in the field of magnonics [33,34]. While a vast amount of fruitful research has provided a good understanding of ferromagnets (FMs) [35–54], analogous studies on antiferromagnets (AFMs) are relatively scarce and have just started appearing [55,56] due to the recently invigorated field of antiferromagnetic spintronics [57–62]. Among the ongoing discoveries of niches borne by AFMs, from electrically and rapidly switchable memories [63], topological spintronics [60], long-range magnonic transport [64], to quantum fluctuations [65], an unexpected surprise has been encountered in the first-principles evaluation of damping in metallic AFMs. Liu and co-workers [56] and another more recent first-principles study [66] both found the magnetization dissipation parameter to be much larger than the corresponding Néel damping constant, in stark contrast with previous assumptions, exhibiting richer features than in FMs. An understanding of this qualitative difference as well as the general AFM dissipation is crucial for the rapidly growing applications and fundamental novel phenomena based on AFMs.

Here, we accomplish an intuitive and general understanding of the Gilbert damping in metallic AFMs based on the magnon picture of AFM dynamics. Employing the *s-d*, two-sublattice model for a metallic AFM, in which the *d* and *s* electrons constitute the magnetic and conduction subsystems, we derive analytic expressions for the Gilbert damping parameters as a function of the conduction electron density of states at the Fermi energy and *s-d* exchange strength. Our analytic results yield values consistent with available numerical studies [56,66] and experiments [67,68]. The presence of spin-degenerate conduction bands in AFMs is found to be the key in their qualitatively different damping properties as compared to FMs. This allows for absorption of AFM magnons via *s-d* exchange-mediated intraband conduction electron spin-flip processes leading to strong damping of the magnetization as compared to the Néel field [69]. We also show that interband spin-flip processes, which are forbidden in our simple AFM model but possible in AFMs with band crossings in the conduction electron dispersion, result in a strong Néel field damping. Thus, the general qualitative features of damping in metallic AFMs demonstrated herein allow us to understand the Gilbert damping given the conduction electron band structure. These insights provide guidance for engineering AFMs with desired damping properties, which depend on the exact role of the AFM in a device.

Model. We consider two-sublattice metallic AFMs within the *s-d* model [35,36,44]. The *d* electrons localized at lattice sites constitute the magnetic subsystem responsible for

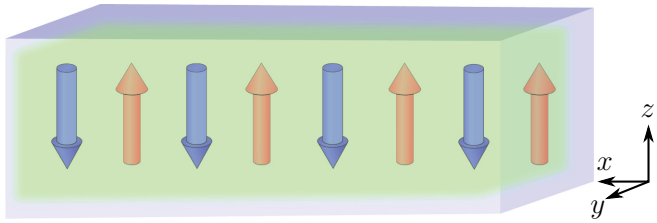

FIG. 1. Schematic depiction of our model for a metallic AFM. The red and blue arrows represent the localized d electrons with spin up and down, and constitute the Néel ordered magnetic subsystems. The green cloud illustrates the delocalized, itinerant s electrons that forms the conduction subsystem.

antiferromagnetism, while the itinerant s electrons form the conduction subsystem that accounts for the metallic traits. The two subsystems interact via s-d exchange [Eq. (3)]. For ease of depiction and enabling an understanding of qualitative trends, we here consider a one-dimensional AFM (Fig. 1). The results within this simple model are generalized to AFMs with any dimensionality in a straightforward manner. Furthermore, we primarily focus on the uniform magnetization dynamics modes.

At each lattice site i, there is a localized d electron with spin $\boldsymbol{S}_i$. The ensuing magnetic subsystem is antiferromagnetically ordered (Fig. 1), and the quantized excitations are magnons [70,71]. Disregarding applied fields for simplicity and assuming an easy-axis anisotropy along the z axis, the magnetic Hamiltonian, $\mathcal{H}_\mathrm{m} = \tilde{J}\sum_{\langle i,j\rangle}\boldsymbol{S}_i\cdot\boldsymbol{S}_j - K\sum_i(S_i^z)^2$, where $\langle i,j\rangle$ denotes summation over nearest-neighbor lattice sites, is quantized and mapped to the sublattice-magnon basis [71]

$$\mathcal{H}_\mathrm{m} = \sum_{\boldsymbol{q}}[A_{\boldsymbol{q}}(a_{\boldsymbol{q}}^\dagger a_{\boldsymbol{q}} + b_{\boldsymbol{q}}^\dagger b_{\boldsymbol{q}}) + B_{\boldsymbol{q}}^\dagger a_{\boldsymbol{q}}^\dagger b_{\boldsymbol{q}}^\dagger + B_{\boldsymbol{q}} a_{\boldsymbol{q}} b_{\boldsymbol{q}}], \quad (1)$$

where we substitute $\hbar = 1$, $A_{\boldsymbol{q}} = (2\tilde{J} + 2K)S$, and $B_{\boldsymbol{q}} = \tilde{J}Se^{-i\boldsymbol{q}\cdot\boldsymbol{a}}\sum_{\langle\boldsymbol{\delta}\rangle}e^{i\boldsymbol{q}\cdot\boldsymbol{\delta}}$, where $S = |\boldsymbol{S}_i|$, $\boldsymbol{a}$ is the displacement between the two atoms in the basis, and $\langle\boldsymbol{\delta}\rangle$ denotes summing over nearest-neighbor displacement vectors. $a_{\boldsymbol{q}}$ and $b_{\boldsymbol{q}}$ are bosonic annihilation operators for plane-wave magnons on the A and B sublattices, respectively. We diagonalize the Hamiltonian [Eq. (1)] through a Bogoliubov transformation [71] to $\mathcal{H}_\mathrm{m} = \sum_{\boldsymbol{q}}\omega_{\boldsymbol{q}}(\alpha_{\boldsymbol{q}}^\dagger\alpha_{\boldsymbol{q}} + \beta_{\boldsymbol{q}}^\dagger\beta_{\boldsymbol{q}})$, with eigenenergies $\omega_{\boldsymbol{q}} = \sqrt{A_{\boldsymbol{q}}^2 - |B_{\boldsymbol{q}}|^2}$. In the absence of an applied field, the magnon modes are degenerate.

The s electron conduction subsystem is described by a tight-binding Hamiltonian that includes the "static" contribution from the s-d exchange interaction [Eq. (3)] discussed below:

$$\mathcal{H}_\mathrm{e} = -t\sum_{\langle i,j\rangle}\sum_\sigma c_{i\sigma}^\dagger c_{j\sigma} - J\sum_i(-1)^i(c_{i\uparrow}^\dagger c_{i\uparrow} - c_{i\downarrow}^\dagger c_{i\downarrow}). \quad (2)$$

Here $c_{i\sigma}$ is the annihilation operator for an s electron at site i with spin σ. t (>0) is the hopping parameter, and J (>0) accounts for s-d exchange interaction [Eq. (3)]. The $(-1)^i$ factor in the exchange term reflects the two-sublattice nature of the AFM. The conduction subsystem unit cell consists

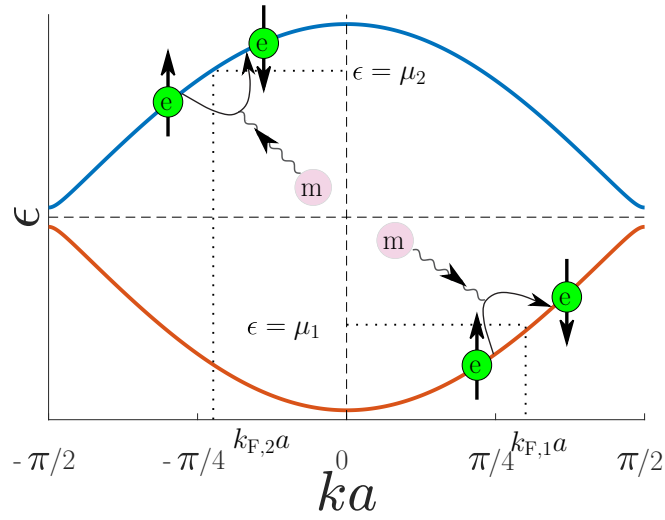

FIG. 2. The s electron dispersion in the metallic AFM model with illustrations of intraband electron-magnon scattering at two different Fermi levels, μ_1 and μ_2. The depicted momentum transfer is exaggerated for clarity.

of two basis atoms, similar to the magnetic subsystem. As a result, there are four distinct electron bands: two due to there being two basis atoms per unit cell, and twice this due to the two possible spin polarizations. Disregarding applied fields, these constitute two spin-degenerate bands. We label these bands 1 and 2, where the latter is higher in energy. The itinerant electron Hamiltonian [Eq. (2)] is diagonalized into an eigenbasis $(c_{1k\sigma}, c_{2k\sigma})$ with eigenenergies $\epsilon_{1k} = -\epsilon_k$ and $\epsilon_{2k} = +\epsilon_k$, where $\epsilon_k = \sqrt{J^2S^2 + t^2|\gamma_k|^2}$, where $\gamma_k = \sum_{\langle\delta\rangle}e^{-ik\cdot\delta}$. The itinerant electron dispersion is depicted in Fig. 2.

The magnetic and conduction subsystems interact through s-d exchange interaction, parametrized by J:

$$\mathcal{H}_\mathrm{I} = -J\sum_i\boldsymbol{S}_i\cdot\boldsymbol{s}_i, \quad (3)$$

where $\boldsymbol{s}_i = \sum_{\sigma\sigma'}c_{i\sigma}^\dagger\boldsymbol{\sigma}_{\sigma\sigma'}c_{i\sigma'}$ is the spin of the itinerant electrons at site i, where $\boldsymbol{\sigma}$ is the vector of Pauli matrices. The term which is zeroth order in the magnon operators, and thus accounts for the static magnetic texture, is already included in $\mathcal{H}_\mathrm{e}$ [Eq. (2)]. To first order in magnon operators, the interaction Hamiltonian can be compactly written as

$$\mathcal{H}_\mathrm{e\text{-}m} = \sum_{\lambda\rho}\sum_{kk'q}c_{\lambda k\uparrow}^\dagger c_{\rho k'\downarrow}\left(W_{kk'q}^{\mathrm{A},\lambda\rho}a_{-q}^\dagger + W_{kk'q}^{\mathrm{B},\lambda\rho}b_q\right) + \mathrm{H.c.}, \quad (4)$$

where λ and ρ are summed over the electron band indices. As detailed in the Supplemental Material [72], $W_{kk'q}^{\mathrm{A},\lambda\rho}$ and $W_{kk'q}^{\mathrm{B},\lambda\rho}$, both linear in J, are coefficients determining the amplitudes for scattering between the itinerant electrons and the a_q and b_q magnons, respectively. Specifically, when considering plane-wave states, $W_{kk'q}^{\mathrm{A/B},\lambda\rho}$ becomes a delta function, thereby enforcing the conservation of crystal momentum in a translationally invariant lattice. Inclusion of disorder or other many-body effects results in deviation of the eigenstates

from ideal plane waves causing a wave vector spread around its mean value [2]. The delta function, associated with an exact crystal momentum conservation, is thus transformed to a peaked function with finite width (Δk). The $\lambda\rho$ combinations 11 and 22 describe *intraband* electron scattering, while 12 and 21 describe *interband* scattering. Intraband scattering is illustrated in Fig. 2.

The scattering described by $\mathcal{H}_{\text{e-m}}$ [Eq. (4)] transfers spin angular momentum between the magnetic and conduction subsystems. The itinerant electrons are assumed to maintain a thermal distribution thereby acting as a perfect spin sink. This is consistent with a strong conduction electron spin relaxation observed in metallic AFMs [73,74]. As a result, the magnetic subsystem spin is effectively damped through the *s-d* exchange interaction.

Gilbert damping. In the LLG phenomenology for two-sublattice AFMs, dissipation is accounted via a 2×2 Gilbert damping matrix [75,76]. Our goal here is to determine the elements of this matrix in terms of the parameters and physical observables within our microscopic model. To this end, we evaluate the spin current "pumped" by the magnetic subsystem into the s conduction electrons, which dissipate the spins immediately within our model. The angular momentum thus lost by the magnetic subsystem appears as Gilbert damping in its dynamical equations [75,77]. The second essential ingredient in identifying the Gilbert damping matrix from our microscopic theory is the idea of coherent states [78,79]. The classical LLG description of the magnetization is necessarily equivalent to our quantum formalism, when the magnetic eigenmode is in a coherent state [78–80]. Driving the magnetization dynamics via a microwave field, such as in the case of ferromagnetic resonance experiments, achieves such a coherent magnetization dynamics [77,81].

The spin current pumped by a two-sublattice magnetic system into an electronic bath may be expressed as [82]

$$\begin{aligned} I_z = {} & G_{mm}(\boldsymbol{m}\times\dot{\boldsymbol{m}})^z + G_{nn}(\boldsymbol{n}\times\dot{\boldsymbol{n}})^z \\ & + G_{mn}[(\boldsymbol{m}\times\dot{\boldsymbol{n}})^z + (\boldsymbol{n}\times\dot{\boldsymbol{m}})^z], \end{aligned} \tag{5}$$

where $\boldsymbol{m}$ and $\boldsymbol{n}$ are the magnetization and Néel field normalized by the sublattice magnetization, respectively. Here, $G_{ij} = \alpha_{ij} \times (M/|\gamma|)$, where α_{ij} are the Gilbert damping coefficients, γ is the gyromagnetic ratio of the d electrons, and M is the sublattice magnetization. Considering the uniform magnetization mode, I_z is the spin current operator $I_z = i[\mathcal{H}_{\text{e-m}}, S^z]$ [83], where $S^z = \sum_i S_i^z$. We get

$$I_z = i\sum_{\lambda\rho}\sum_{\boldsymbol{k}\boldsymbol{k}'\boldsymbol{q}}\left\{c^\dagger_{\lambda\boldsymbol{k}\uparrow}c_{\rho\boldsymbol{k}'\downarrow}\left(W^{\text{A},\lambda\rho}_{\boldsymbol{k}\boldsymbol{k}'\boldsymbol{q}}a^\dagger_{-\boldsymbol{q}} + W^{\text{B},\lambda\rho}_{\boldsymbol{k}\boldsymbol{k}'\boldsymbol{q}}b_{\boldsymbol{q}}\right) - \text{H.c.}\right\}. \tag{6}$$

The expectation value of this operator assuming the uniform magnetization mode to be in a coherent state corresponds to the spin pumping current [Eq. (5)].

In order to evaluate the spin pumping current from Eq. (6), we follow the method employed to calculate interfacial spin pumping current into normal metals in Refs. [77,81,82], and the procedure is described in detail therein. Briefly, this method entails assuming the magnetic and conduction subsystems to be independent and in equilibrium at $t = -\infty$, when the mutual interaction [Eq. (4)] is turned on. The subsequent time evolution of the coupled system allows evaluating its physical observables in steady state. The resulting coherent spin current corresponds to the classical spin current I_z that can be related to the motion of the magnetization and the Néel field [Eq. (5)]. As a last step, we identify expressions for $(\boldsymbol{m}\times\dot{\boldsymbol{m}})^z$, $(\boldsymbol{m}\times\dot{\boldsymbol{n}})^z$, and $(\boldsymbol{n}\times\dot{\boldsymbol{n}})^z$ in terms of coherent magnon states, which enables us to identify the Gilbert damping coefficients α_{mm}, α_{nn}, and α_{mn}.

Results. Relegating the detailed evaluation to Supplemental Material [72], we now present the analytic expression obtained for the various coefficients [Eq. (5)]. A key assumption that allows these simple expressions is that the electronic density of states in the conduction subsystem does not vary significantly over the magnon energy scale. Furthermore, we account for a weak disorder phenomenologically via a finite scattering length l associated with the conduction electrons. This results in an effective broadening of the electron wave vectors determined by the inverse electron scattering length, $(\Delta k) = 2\pi/l$. As a result, the crystal momentum conservation in the system is enforced only within the wave vector broadening. By weak disorder we mean that the electron scattering length is much larger than the lattice parameter a. If k and k' are the wave vectors of the incoming and outgoing electrons, respectively, we then have $(k-k')a = (\Delta k)a \ll 1$. This justifies an expansion in the wave vector broadening $(\Delta k)a$. The Gilbert damping coefficients stemming from intraband electron scattering are found to be

$$\begin{aligned} \alpha_{mm} = {} & \alpha_0(\xi_J) \\ & - \frac{\alpha_0(\xi_J)}{4}\left(1 + \frac{\xi_J^2\left[\xi_J^2 + 8 - 4\cos^2(k_{\text{F}}a)\right]}{\left[\xi_J^2 + 4\cos^2(k_{\text{F}}a)\right]^2}\right)[(\Delta k)a]^2, \\ \alpha_{nn} = {} & \frac{\alpha_0(\xi_J)}{4}\left(1 + \frac{\sin^2(k_{\text{F}}a)}{\cos^2(k_{\text{F}}a)}\frac{\xi_J^2}{\left[\xi_J^2 + 4\cos^2(k_{\text{F}}a)\right]}\right)[(\Delta k)a]^2, \end{aligned} \tag{7}$$

where $\xi_J = JS/t$, k_{F} is the Fermi momentum, and a is the lattice parameter, and where

$$\alpha_0(\xi_J) = \frac{\pi v^2 J^2}{2} g^2(\mu)|\tilde{V}|^2 \frac{4\cos^2(k_{\text{F}}a)}{\xi_J^2 + 4\cos^2(k_{\text{F}}a)}. \tag{8}$$

$\alpha_{mn} = \alpha_{nm} = 0$ due to the equivalence between the two sublattices [75] in an AFM. Here, v is the unit cell volume, $g(\epsilon)$ is the density of states per unit volume, μ is the Fermi level, and ω_0 is the energy of the $\boldsymbol{q} = \boldsymbol{0}$ magnon mode. $\tilde{V}$ is a dimensionless and generally complex function introduced to account for the momentum broadening dependency of the scattering amplitudes. It satisfies $\tilde{V}(0) = 1$ and $0 \leqslant |\tilde{V}(\Delta k)| \leqslant 1$ within our model. These analytic expressions for the Gilbert damping parameters constitute one of the main results of this Rapid Communication.

Discussion. The Gilbert damping in metallic AFMs [Eq. (7)] bears dependencies similar to the analogous case of spin pumping in AFM|NM bilayers with interfacial exchange coupling [82]. There are, however, two key differences: The *s-d* exchange coupling exists in the bulk of metallic AFMs, whereas it is localized at the interface in the bilayer structures. Additionally, the itinerant electron wave functions follow

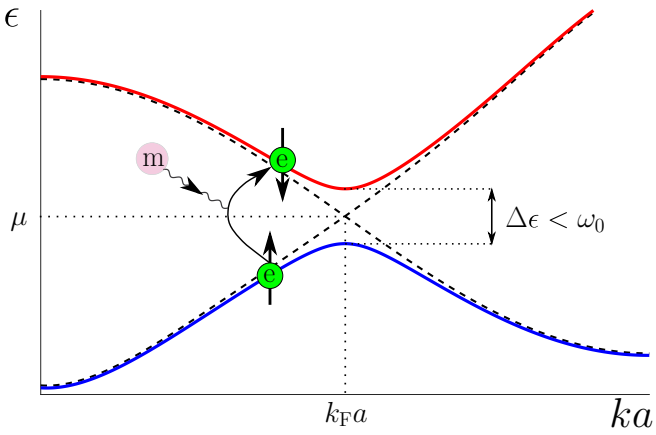

FIG. 3. A schematic depiction of magnon-induced interband scattering in a band (anti-)crossing at the Fermi level.

distinct periodicities in metallic AFMs [72], FMs and NMs, amounting to qualitative differences.

In the limit of weak momentum broadening $(\Delta k)a \ll 1$ and weak *s-d* exchange $\xi_J \ll 1$, we arrive at $\alpha_{nn} \approx 0$ and $\alpha_{mm} = \pi v^2 J^2 g^2(\mu)/2$ for intraband scattering. In this experimentally relevant limit we need only two material input parameters, J and $g(\mu)$, to compute the Gilbert damping. Using a typical value of $J \sim 0.1$ eV [36], and density of states from a selection of experiments and density functional theory (DFT) calculations [84–88], we obtain α_{mm} comparable to the first-principles calculation results [56,66] (see Supplemental Material [72] for details). For instance, we find that $\alpha_{mm} = 0.35$ in FeMn, while the DFT calculation in Ref. [56] finds $\alpha_{mm} = 0.38$. Moreover, experiments in $Mn_{90}Cu_{10}$ imply $\alpha_{mm} = 0.3$ [67,68]. Since the relevant material parameters are not available in $Mn_{90}Cu_{10}$, we assume a $g(\mu)$ similar to other manganese-based AFMs, e.g., IrMn, and obtain $\alpha_{mm} = 0.14$.

The uniform mode magnon energy is much smaller than the electron band gap within our simple model, prohibiting interband scattering. However, in real AFM metals with more complex band structures, band crossings with gaps smaller than the magnon energy may exist [89–91]. In materials with band crossings at the Fermi level, magnon-induced interband scattering should also contribute to Gilbert damping. Motivated by this, we now consider Gilbert damping stemming from interband scattering within the minimal model, while disregarding the energy conservation for the moment, labeling the coefficients α^I_{mm} and α^I_{nn}. We then find the same expressions as in Eq. (7) with the roles of $\alpha^I_{mm,nn}$ interchanged with respect to $\alpha_{mm,nn}$, giving a non-negligible α^I_{nn}. Although arriving at this result required disregarding energy conservation, the qualitative effect in itself is not an artifact of this. For Gilbert damping resulting from band (anti-)crossings (with band gap $\Delta\epsilon < \omega_0$) as depicted in Fig. 3, $\alpha^I_{nn}/\alpha^I_{mm} \gtrsim \alpha_{nn}/\alpha_{mm}$. This generic principle derived within our simple model provides valuable guidance for designing materials with an engineered Gilbert damping matrix.

We now provide a rough intuitive picture for the damping dependencies obtained above followed by a more mathematical discussion. Consider a conventional diffraction experiment where an incident probing wave is able to resolve the two slits only when the wavelength is comparable to the physical separation between the two slits. In the case at hand, the wave functions of electrons and magnons participating in a scattering process combine in a way that the wave number by which the conservation of crystal momentum is violated becomes the probing wave number within a diffraction picture. Therefore, the processes conserving crystal momentum have vanishing probing wave number and are not able to resolve the opposite spins localized at adjacent lattice sites. Therefore, only the average magnetization is damped leaving the Néel field unaffected. With disorder, the probing wave number becomes nonzero and thus also couples to the Néel field. The interband scattering, on the other hand, is reminiscent of umklapp scattering in a single-sublattice model and the probing wave number matches with the inverse lattice spacing. Therefore, the coupling with the Néel field is strong.

The Gilbert damping in metallic AFMs here considered is caused by spin pumping from the magnetic subsystem into the *s* band, and depends thus on transition amplitudes proportional to products of itinerant electron wave functions such as $\psi^\dagger_{\lambda k\uparrow}(x)\psi_{\rho k'\downarrow}(x)$. The damping on sublattices A and B is therefore a function of $\sum_j \cos^2(\frac{\pi x_j}{2a})\psi^\dagger_{\lambda k\uparrow}(x_j)\psi_{\rho k'\downarrow}(x_j)$ and $\sum_j \sin^2(\frac{\pi x_j}{2a})\psi^\dagger_{\lambda k\uparrow}(x_j)\psi_{\rho k'\downarrow}(x_j)$, respectively. Equivalently, α_{mm} is a function of $\sum_j \psi^\dagger_{\lambda k\uparrow}(x_j)\psi_{\rho k'\downarrow}(x)$, and α_{nn} is a function of $\sum_j \cos(\frac{\pi x_j}{a})\psi^\dagger_{\lambda k\uparrow}(x_j)\psi_{\rho k'\downarrow}(x)$. Assuming plane-wave solutions of the electron wave functions, considering intraband scattering only, we find that α_{mm} is a function of $[1 - i(\Delta k)a]$, where i is the imaginary unit, whereas α_{nn} is a function of $(\Delta k)a$. This coincides well with Eq. (7). In the limit of a negligible band gap in the simple model presented previously, the upper electron band is a continuation of the lower band with a $\pm\pi/a$ momentum shift. Therefore, interband scattering at momentum k is equivalent to intraband scattering between k and $k \pm \pi/a$. This is indeed the exact phase shift which results in a large α_{nn}.

The magnon decay picture developed herein goes beyond metals, where electron-magnon scattering constitutes the dominant mechanism for magnon decay and thus Gilbert damping. In insulators, magnon-phonon and magnon-magnon scattering provide comparable competing damping channels. The present methodology can thus be generalized to insulators. From an experimental perspective, magnetic resonance linewidth measurement has been a standard approach to extracting Gilbert damping. Recent studies [55] have employed terahertz spectroscopy as a means of studying damping in AFMs, while time-resolved magnetization dynamics offers further possibilities [92,93]. As regards corroborating and exploiting our finding of interband scattering effects, a way to control the degree of interband scattering at the Fermi level will be helpful in isolating its contribution. This may be achieved by doping an antiferromagnet in which a band crossing is close to the Fermi level [89–91], and investigating the Gilbert damping as a function of doping.

Conclusion. We have provided a microscopic derivation of Gilbert damping resulting from magnon decay through *s-d* exchange interaction in metallic antiferromagnets. Analytic expressions for Gilbert damping coefficients resulting from

intraband electron scattering are presented, while Gilbert damping resulting from interband electron scattering is discussed on a conceptual level. We find that intraband electron scattering gives rise to a large magnetization damping and a negligible Néel field damping. The intraband Néel field damping is proportional to the inverse electron scattering length squared, and disappears exactly if there is no crystal disorder. By relating Gilbert damping to the degree to which transition amplitudes of the itinerant electron are in phase at neighboring lattice sites, we have argued for why interband electron scattering may generate a large Néel field damping.

Acknowledgments. This work was supported by the Research Council of Norway through its Centres of Excellence funding scheme, Project No. 262633 "QuSpin," the European Union's Horizon 2020 Research and Innovation Programme under Grant No. DLV-737038 "TRANSPIRE," as well as by the European Research Council via Advanced Grant No. 669442 "Insulatronics."

[1] R. P. Feynman and F. L. Vernon, The theory of a general quantum system interacting with a linear dissipative system, Ann. Phys. (NY) **24**, 118 (1963).

[2] G. D. Mahan, *Many-Particle Physics*, 3rd ed. (Kluwer Academic/Plenum Publishers, New York, 2000).

[3] A. O. Caldeira and A. J. Leggett, Influence of Dissipation on Quantum Tunneling in Macroscopic Systems, Phys. Rev. Lett. **46**, 211 (1981).

[4] A. V. Kimel, A. Kirilyuk, A. Tsvetkov, R. V. Pisarev, and T. Rasing, Laser-induced ultrafast spin reorientation in the antiferromagnet $TmFeO_3$, Nature (London) **429**, 850 (2004).

[5] A. Kirilyuk, A. V. Kimel, and T. Rasing, "Ultrafast optical manipulation of magnetic order," Rev. Mod. Phys. **82**, 2731 (2010).

[6] A. Brataas, A. D. Kent, and H. Ohno, Current-induced torques in magnetic materials, Nat. Mater. **11**, 372 (2012).

[7] R. Fazio and H. van der Zant, Quantum phase transitions and vortex dynamics in superconducting networks, Phys. Rep. **355**, 235 (2001).

[8] A. Biella, L. Mazza, I. Carusotto, D. Rossini, and R. Fazio, Photon transport in a dissipative chain of nonlinear cavities, Phys. Rev. A **91**, 053815 (2015).

[9] D. Maile, S. Andergassen, W. Belzig, and G. Rastelli, Quantum phase transition with dissipative frustration, Phys. Rev. B **97**, 155427 (2018).

[10] G. Rastelli and I. M. Pop, Tunable ohmic environment using Josephson junction chains, Phys. Rev. B **97**, 205429 (2018).

[11] C. Kittel, Interaction of Spin Waves and Ultrasonic Waves in Ferromagnetic Crystals, Phys. Rev. **110**, 836 (1958).

[12] M. Weiler, H. Huebl, F. S. Goerg, F. D. Czeschka, R. Gross, and S. T. B. Goennenwein, Spin Pumping with Coherent Elastic Waves, Phys. Rev. Lett. **108**, 176601 (2012).

[13] A. Rückriegel, P. Kopietz, D. A. Bozhko, A. A. Serga, and B. Hillebrands, Magnetoelastic modes and lifetime of magnons in thin yttrium iron garnet films, Phys. Rev. B **89**, 184413 (2014).

[14] A. Kamra, H. Keshtgar, P. Yan, and G. E. W. Bauer, Coherent elastic excitation of spin waves, Phys. Rev. B **91**, 104409 (2015).

[15] B. Flebus, K. Shen, T. Kikkawa, K.-i. Uchida, Z. Qiu, E. Saitoh, R. A. Duine, and G. E. W. Bauer, Magnon-polaron transport in magnetic insulators, Phys. Rev. B **95**, 144420 (2017).

[16] T. Kikkawa, K. Shen, B. Flebus, R. A. Duine, K.-i. Uchida, Z. Qiu, G. E. W. Bauer, and E. Saitoh, Magnon Polarons in the Spin Seebeck Effect, Phys. Rev. Lett. **117**, 207203 (2016).

[17] L. Dreher, M. Weiler, M. Pernpeintner, H. Huebl, R. Gross, M. S. Brandt, and S. T. B. Goennenwein, Surface acoustic wave driven ferromagnetic resonance in nickel thin films: Theory and experiment, Phys. Rev. B **86**, 134415 (2012).

[18] H. T. Simensen, R. E. Troncoso, A. Kamra, and A. Brataas, Magnon-polarons in cubic collinear antiferromagnets, Phys. Rev. B **99**, 064421 (2019).

[19] H. Huebl, C. W. Zollitsch, J. Lotze, F. Hocke, M. Greifenstein, A. Marx, R. Gross, and S. T. B. Goennenwein, High Cooperativity in Coupled Microwave Resonator Ferrimagnetic Insulator Hybrids, Phys. Rev. Lett. **111**, 127003 (2013).

[20] Y. Tabuchi, S. Ishino, A. Noguchi, T. Ishikawa, R. Yamazaki, K. Usami, and Y. Nakamura, Coherent coupling between a ferromagnetic magnon and a superconducting qubit, Science **349**, 405 (2015).

[21] C. Hu, B. M. Yao, S. Kaur, Y. S. Gui, and W. Lu, Magnon polariton and pseudo-magnon-polariton, in *2015 40th International Conference on Infrared, Millimeter, and Terahertz Waves (IRMMW-THz)* (IEEE, Hong Kong, China, 2015), pp. 1–3.

[22] Ø. Johansen and A. Brataas, Nonlocal Coupling between Antiferromagnets and Ferromagnets in Cavities, Phys. Rev. Lett. **121**, 087204 (2018).

[23] M. Harder and C.-M. Hu, Cavity Spintronics: An Early Review of Recent Progress in the Study of Magnon-Photon Level Repulsion, in *Solid State Physics 69*, edited by R. E. Camley and R. L. Stamps (Academic, Cambridge, 2018), pp. 47–121.

[24] Y. Cao, P. Yan, H. Huebl, S. T. B. Goennenwein, and G. E. W. Bauer, Exchange magnon-polaritons in microwave cavities, Phys. Rev. B **91**, 094423 (2015).

[25] A. Frisk Kockum, A. Miranowicz, S. De Liberato, S. Savasta, and F. Nori, Ultrastrong coupling between light and matter, Nat. Rev. Phys. **1**, 19 (2019).

[26] J. Holanda, D. S. Maior, A. Azevedo, and S. M. Rezende, Detecting the phonon spin in magnon-phonon conversion experiments, Nat. Phys. **14**, 500 (2018).

[27] S. Viola Kusminskiy, H. X. Tang, and F. Marquardt, Coupled spin-light dynamics in cavity optomagnonics, Phys. Rev. A **94**, 033821 (2016).

[28] N. Samkharadze, G. Zheng, N. Kalhor, D. Brousse, A. Sammak, U. C. Mendes, A. Blais, G. Scappucci, and L. M. K. Vandersypen, Strong spin-photon coupling in silicon, Science **359**, 1123 (2018).

[29] M. Harder, Y. Yang, B. M. Yao, C. H. Yu, J. W. Rao, Y. S. Gui, R. L. Stamps, and C.-M. Hu, Level Attraction Due to Dissipative Magnon-Photon Coupling, Phys. Rev. Lett. **121**, 137203 (2018).

[30] P. F. Herskind, A. Dantan, J. P. Marler, M. Albert, and M. Drewsen, Realization of collective strong coupling with ion Coulomb crystals in an optical cavity, Nat. Phys. **5**, 494 (2009).

[31] L. D. Landau and E. Lifshitz, On the theory of the dispersion of magnetic permeability in ferromagnetic bodies, Phys. Z. Sowjet. **8**, 153 (1935).

[32] T. Gilbert, Classics in magnetics: A phenomenological theory of damping in ferromagnetic materials, IEEE Trans. Magn. **40**, 3443 (2004).
[33] V. V. Kruglyak, S. O. Demokritov, and D. Grundler, Magnonics, J. Phys. D **43**, 264001 (2010).
[34] A. V. Chumak, V. I. Vasyuchka, A. A. Serga, and B. Hillebrands, Magnon spintronics, Nat. Phys. **11**, 453 (2015).
[35] A. H. Mitchell, Ferromagnetic Relaxation by the Exchange Interaction between Ferromagnetic Electrons and Conduction Electrons, Phys. Rev. **105**, 1439 (1957).
[36] B. Heinrich, D. Fraitová, and V. Kamberský, The Influence of *s-d* Exchange on Relaxation of Magnons in Metals, Phys. Status Solidi B **23**, 501 (1967).
[37] V. Kamberský, On the Landau-Lifshitz relaxation in ferromagnetic metals, Can. J. Phys. **48**, 2906 (1970).
[38] V. Kamberský, On ferromagnetic resonance damping in metals, Czech. J. Phys. **26**, 1366 (1976).
[39] J. Kuneš and V. Kamberský, First-principles investigation of the damping of fast magnetization precession in ferromagnetic 3*d* metals, Phys. Rev. B **65**, 212411 (2002).
[40] A. Y. Dobin and R. H. Victora, Intrinsic Nonlinear Ferromagnetic Relaxation in Thin Metallic Films, Phys. Rev. Lett. **90**, 167203 (2003).
[41] S. Zhang and Z. Li, Roles of Nonequilibrium Conduction Electrons on the Magnetization Dynamics of Ferromagnets, Phys. Rev. Lett. **93**, 127204 (2004).
[42] Y. Tserkovnyak, G. A. Fiete, and B. I. Halperin, Mean-field magnetization relaxation in conducting ferromagnets, Appl. Phys. Lett. **84**, 5234 (2004).
[43] V. Kamberský, Spin-orbital Gilbert damping in common magnetic metals, Phys. Rev. B **76**, 134416 (2007).
[44] H. J. Skadsem, Y. Tserkovnyak, A. Brataas, and G. E. W. Bauer, Magnetization damping in a local-density approximation, Phys. Rev. B **75**, 094416 (2007).
[45] K. Gilmore, Y. U. Idzerda, and M. D. Stiles, Identification of the Dominant Precession-Damping Mechanism in Fe, Co, and Ni by First-Principles Calculations, Phys. Rev. Lett. **99**, 027204 (2007).
[46] A. Brataas, Y. Tserkovnyak, and G. E. W. Bauer, Scattering Theory of Gilbert Damping, Phys. Rev. Lett. **101**, 037207 (2008).
[47] M. C. Hickey and J. S. Moodera, Origin of Intrinsic Gilbert Damping, Phys. Rev. Lett. **102**, 137601 (2009).
[48] A. A. Starikov, P. J. Kelly, A. Brataas, Y. Tserkovnyak, and G. E. W. Bauer, Unified First-Principles Study of Gilbert Damping, Spin-Flip Diffusion, and Resistivity in Transition Metal Alloys, Phys. Rev. Lett. **105**, 236601 (2010).
[49] S. Mankovsky, D. Ködderitzsch, G. Woltersdorf, and H. Ebert, First-principles calculation of the Gilbert damping parameter via the linear response formalism with application to magnetic transition metals and alloys, Phys. Rev. B **87**, 014430 (2013).
[50] Z. Yuan, K. M. D. Hals, Y. Liu, A. A. Starikov, A. Brataas, and P. J. Kelly, Gilbert Damping in Noncollinear Ferromagnets, Phys. Rev. Lett. **113**, 266603 (2014).
[51] E. Barati, M. Cinal, D. M. Edwards, and A. Umerski, Gilbert damping in magnetic layered systems, Phys. Rev. B **90**, 014420 (2014).
[52] F. Mahfouzi, J. Kim, and N. Kioussis, Intrinsic damping phenomena from quantum to classical magnets: An *ab initio* study of Gilbert damping in a Pt/Co bilayer, Phys. Rev. B **96**, 214421 (2017).
[53] Y. Zhao, Y. Liu, H. Tang, H. Jiang, Z. Yuan, and K. Xia, Gilbert damping in FeCo alloy: From weak to strong spin disorder, Phys. Rev. B **98**, 174412 (2018).
[54] Y. Li, F. Zeng, Steven S.-L. Zhang, H. Shin, H. Saglam, V. Karakas, O. Ozatay, J. E. Pearson, O. G. Heinonen, Y. Wu, A. Hoffmann, and W. Zhang, Giant Anisotropy of Gilbert Damping in Epitaxial CoFe Films, Phys. Rev. Lett. **122**, 117203 (2019).
[55] T. Moriyama, K. Hayashi, K. Yamada, M. Shima, Y. Ohya, and T. Ono, Intrinsic and extrinsic antiferromagnetic damping in NiO, Phys. Rev. Mater. **3**, 51402 (2019).
[56] Q. Liu, H. Y. Yuan, K. Xia, and Z. Yuan, Mode-dependent damping in metallic antiferromagnets due to intersublattice spin pumping, Phys. Rev. Mater. **1**, 061401 (2017).
[57] T. Jungwirth, X. Marti, P. Wadley, and J. Wunderlich, Antiferromagnetic spintronics, Nat. Nanotechnol. **11**, 231 (2016).
[58] V. Baltz, A. Manchon, M. Tsoi, T. Moriyama, T. Ono, and Y. Tserkovnyak, Antiferromagnetic spintronics, Rev. Mod. Phys. **90**, 015005 (2018).
[59] A. H. MacDonald and M. Tsoi, Antiferromagnetic metal spintronics, Philos. Trans. R. Soc., A **369**, 3098 (2011).
[60] L. Šmejkal, Y. Mokrousov, B. Yan, and A. H. MacDonald, Topological antiferromagnetic spintronics, Nat. Phys. **14**, 242 (2018).
[61] E. V. Gomonay and V. M. Loktev, Spintronics of antiferromagnetic systems (Review Article), Low Temp. Phys. **40**, 17 (2014).
[62] O. Gomonay, V. Baltz, A. Brataas, and Y. Tserkovnyak, Antiferromagnetic spin textures and dynamics, Nat. Phys. **14**, 213 (2018).
[63] P. Wadley, B. Howells, J. Elezny, C. Andrews, V. Hills, R. P. Campion, V. Novak, K. Olejnik, F. Maccherozzi, S. S. Dhesi, S. Y. Martin, T. Wagner, J. Wunderlich, F. Freimuth, Y. Mokrousov, J. Kune, J. S. Chauhan, M. J. Grzybowski, A. W. Rushforth, K. W. Edmonds, B. L. Gallagher, and T. Jungwirth, Electrical switching of an antiferromagnet, Science **351**, 587 (2016).
[64] R. Lebrun, A. Ross, S. A. Bender, A. Qaiumzadeh, L. Baldrati, J. Cramer, A. Brataas, R. A. Duine, and M. Kläui, Tunable long-distance spin transport in a crystalline antiferromagnetic iron oxide, Nature (London) **561**, 222 (2018).
[65] A. Kamra, E. Thingstad, G. Rastelli, R. A. Duine, A. Brataas, W. Belzig, and A. Sudbø, Antiferromagnetic magnons as highly squeezed Fock states underlying quantum correlations, Phys. Rev. B **100**, 174407 (2019).
[66] F. Mahfouzi and N. Kioussis, Damping and antidamping phenomena in metallic antiferromagnets: An *ab initio* study, Phys. Rev. B **98**, 220410(R) (2018).
[67] M. C. K. Wiltshire and M. M. Elcombe, Temperature dependence of magnons in γ-MnCu, J. Magn. Magn. Mater. **31–34**, 127 (1983).
[68] J. A. Fernandez-Baca, M. E. Hagen, R. M. Nicklow, Y. Tsunoda, and S. M. Hayden, Magnetic excitations in the itinerant antiferromagnet $Mn_{90}Cu_{10}$, J. Magn. Magn. Mater. **104–107**, 699 (1992).
[69] Such processes are forbidden in ferromagnets due to spin splitting between the opposite spin conduction electron bands.
[70] P. W. Anderson, An Approximate Quantum Theory of the Antiferromagnetic Ground State, Phys. Rev. **86**, 694 (1952).

[71] R. Kubo, The Spin-Wave Theory of Antiferromagnetics, Phys. Rev. **87**, 568 (1952).

[72] See Supplemental Material at http://link.aps.org/supplemental/10.1103/PhysRevB.101.020403 for a detailed derivation of the electron modes in metallic antiferromagnets, the scattering amplitudes between magnons and electrons due to *s-d* exchange interaction, a derivation of the Gilbert damping parameters due to magnon decay through *s-d* exchange interaction, and a comparison between our analytic results and values obtained via first-principles calculations as well as experiments.

[73] P. Merodio, A. Ghosh, C. Lemonias, E. Gautier, U. Ebels, M. Chshiev, H. Béa, V. Baltz, and W. E. Bailey, Penetration depth and absorption mechanisms of spin currents in $Ir_{20}Mn_{80}$ and $Fe_{50}Mn_{50}$ polycrystalline films by ferromagnetic resonance and spin pumping, Appl. Phys. Lett. **104**, 032406 (2014).

[74] L. Frangou, S. Oyarzún, S. Auffret, L. Vila, S. Gambarelli, and V. Baltz, Enhanced Spin Pumping Efficiency in Antiferromagnetic IrMn Thin Films around the Magnetic Phase Transition, Phys. Rev. Lett. **116**, 077203 (2016).

[75] A. Kamra, R. E. Troncoso, W. Belzig, and A. Brataas, Gilbert damping phenomenology for two-sublattice magnets, Phys. Rev. B **98**, 184402 (2018).

[76] H. Y. Yuan, Q. Liu, K. Xia, Z. Yuan, and X. R. Wang, Proper dissipative torques in antiferromagnetic dynamics, Europhys. Lett. **126**, 67006 (2019).

[77] A. Kamra and W. Belzig, Super-Poissonian Shot Noise of Squeezed-Magnon Mediated Spin Transport, Phys. Rev. Lett. **116**, 146601 (2016).

[78] R. J. Glauber, The Quantum Theory of Optical Coherence, Phys. Rev. **130**, 2529 (1963).

[79] E. C. G. Sudarshan, Equivalence of Semiclassical and Quantum Mechanical Descriptions of Statistical Light Beams, Phys. Rev. Lett. **10**, 277 (1963).

[80] N. Zagury and S. M. Rezende, Theory of macroscopic excitations of magnons, Phys. Rev. B **4**, 201 (1971).

[81] A. Kamra and W. Belzig, Magnon-mediated spin current noise in ferromagnet | nonmagnetic conductor hybrids, Phys. Rev. B **94**, 014419 (2016).

[82] A. Kamra and W. Belzig, Spin Pumping and Shot Noise in Ferrimagnets: Bridging Ferro- and Antiferromagnets, Phys. Rev. Lett. **119**, 197201 (2017).

[83] S. A. Bender and Y. Tserkovnyak, Interfacial spin and heat transfer between metals and magnetic insulators, Phys. Rev. B **91**, 140402(R) (2015).

[84] A. Sakuma, First-principles study on the non-collinear magnetic structures of disordered alloys, J. Phys. Soc. Jpn. **69**, 3072 (2000).

[85] R. Umetsu, K. Fukamichi, and A. Sakuma, Electrical and calorimetric evidences of a pseudo-gap in antiferromagnetic equiatomic MnPd alloy, J. Magn. Magn. Mater. **239**, 530 (2002).

[86] R. Y. Umetsu, M. Miyakawa, K. Fukamichi, and A. Sakuma, Pseudogap in the density of states and the highest Néel temperature of the $L1_0$-type MnIr alloy system, Phys. Rev. B **69**, 104411 (2004).

[87] R. Y. Umetsu, K. Fukamichi, and A. Sakuma, Electronic structures and magnetic phase stability of $L1_0$ and $B2$-type MnRh equiatomic alloys, J. Phys. Soc. Jpn. **76**, 104712 (2007).

[88] L. M. Sandratskii and P. Mavropoulos, Magnetic excitations and femtomagnetism of FeRh: A first-principles study, Phys. Rev. B **83**, 174408 (2011).

[89] P. Tang, Q. Zhou, G. Xu, and S.-c. Zhang, Dirac fermions in an antiferromagnetic semimetal, Nat. Phys. **12**, 1100 (2016).

[90] S. Y. Bodnar, L. Šmejkal, I. Turek, T. Jungwirth, O. Gomonay, J. Sinova, A. A. Sapozhnik, H.-J. Elmers, M. Kläui, and M. Jourdan, Writing and reading antiferromagnetic Mn_2Au by Néel spin-orbit torques and large anisotropic magnetoresistance, Nat. Commun. **9**, 348 (2018).

[91] D. F. Shao, G. Gurung, S. H. Zhang, and E. Y. Tsymbal, Dirac Nodal Line Metal for Topological Antiferromagnetic Spintronics, Phys. Rev. Lett. **122**, 077203 (2019).

[92] Z. Wang, S. Kovalev, N. Awari, M. Chen, S. Germanskiy, B. Green, J.-C. Deinert, T. Kampfrath, J. Milano, and M. Gensch, Magnetic field dependence of antiferromagnetic resonance in NiO, Appl. Phys. Lett. **112**, 252404 (2018).

[93] J. Walowski and M. Münzenberg, Perspective: Ultrafast magnetism and THz spintronics, J. Appl. Phys. **120**, 140901 (2016).